Methane production related to microbiota in dairy cattle feces

Jian Liu, Meng Zhou, Lifeng Zhou, Run Dang, Leilei Xiao, Yang Tan, Meng Li, Jiafeng Yu, Peng Zhang, Marcela Hernández, Eric Lichtfouse

PII: S0013-9351(24)02546-5

DOI: https://doi.org/10.1016/j.envres.2024.120642

Reference: YENRS 120642

To appear in: *Environmental Research*

Received Date: 5 October 2024

Revised Date: 12 December 2024

Accepted Date: 13 December 2024

Please cite this article as: Liu, J., Zhou, M., Zhou, L., Dang, R., Xiao, L., Tan, Y., Li, M., Yu, J., Zhang, P., Hernández, M., Lichtfouse, E., Methane production related to microbiota in dairy cattle feces, *Environmental Research*, https://doi.org/10.1016/j.envres.2024.120642.

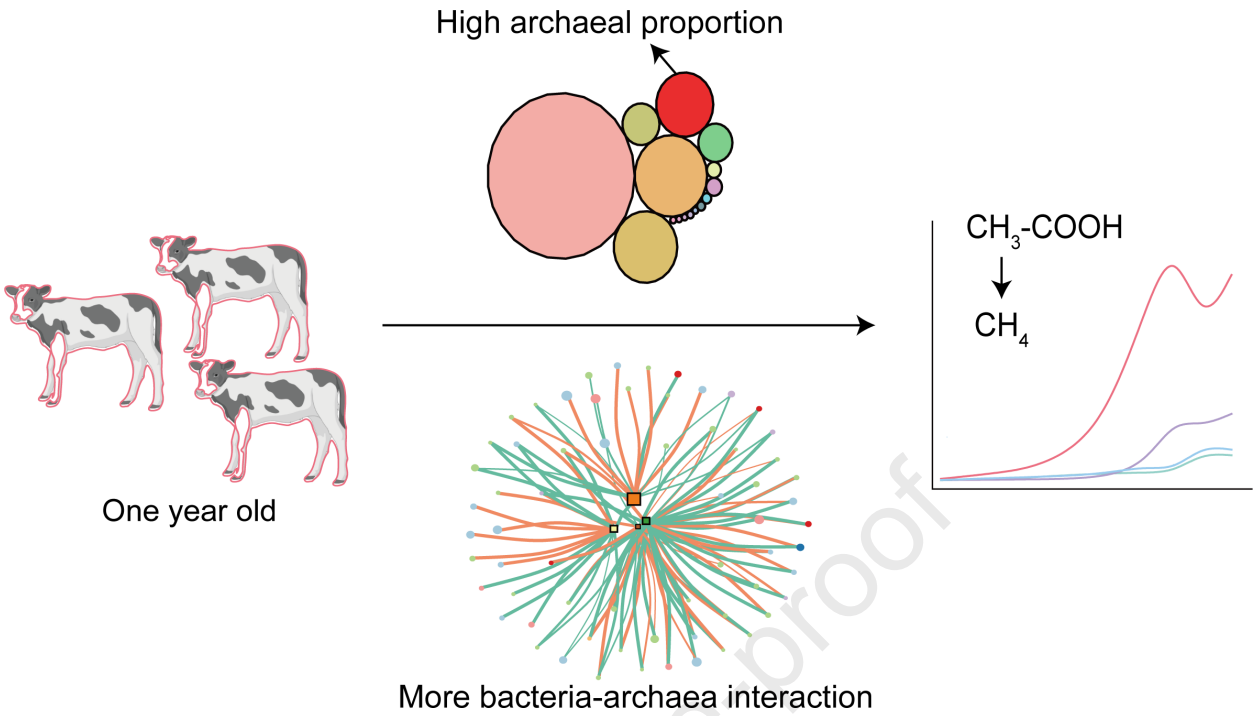

Methane production related to microbiota in dairy cattle feces

Jian Liu [a,d], Meng Zhou [b*], Lifeng Zhou [c,e], Run Dang [c,e], Leilei Xiao [c], Yang Tan [c], Meng Li [a,d], Jiafeng Yu [a,d*], Peng Zhang [f], Marcela Hernández [g], Eric Lichtfouse [h]

[a] Shandong Key Laboratory of Biophysics, Institute of Biophysics, Dezhou University, Dezhou, 253023, P.R. China

[b] State Key Laboratory of Black Soils Conservation and Utilization, Northeast Institute of Geography and Agroecology, Chinese Academy of Sciences, Harbin 150081, P.R. China

[c] CAS Key Laboratory of Coastal Environmental Processes and Ecological Remediation, Yantai Institute of Coastal Zone Research, Chinese Academy of Sciences, Yantai 264003, P.R. China

[d] International Joint Laboratory of Agricultural Food Science and Technology of Universities of Shandong, Dezhou university, Dezhou, 253023, P.R. China

[e] Liaocheng University school of Geography and Environment, Liaocheng, 252059, P.R. China;

[f] Faculty of Environmental Science & Engineering, Kunming University of Science & Technology, Kunming 650500, Yunnan, China

[g] School of Biological Sciences, University of East Anglia, Norwich NR4 7TJ, UK.

[h] State Key Laboratory of Multiphase Flow in Power Engineering, Xi'an Jiaotong University, Xi'an, 710049, Shaanxi, China

[*]**Correspondence:**

State Key Laboratory of Black Soils Conservation and Utilization, Northeast Institute of Geography and Agroecology, Chinese Academy of Sciences, No. 138 Haping Rd.,

Harbin 150081, P.R. China.

Office: +86-0451-86603115, E-mail: zhoumeng@iga.ac.cn

Jiafeng Yu, Shandong Key Laboratory of Biophysics, Institute of Biophysics, Dezhou University, No. 566 University Rd. West, Dezhou 253023, P.R. China.

Office: +86-0534-8982557, E-mail: jfyu1979@dzu.edu.cn

Abstract

Methane (CH_4) emission from livestock feces, led by ruminants, shows a profound impact on global warming. Despite this, we have almost no information on the syntrophy of the intact microbiome metabolisms, from carbohydrates to the one-carbon units, covering multiple stages of ruminant development. In this study, syntrophic effects of polysaccharide degradation and acetate-producing bacteria, and methanogenic archaea were revealed through metagenome-assembled genomes from water saturated dairy cattle feces. Although CH_4 is thought to be produced by archaea, more edges, nodes, and balanced interaction types revealed by network analysis provided a closed bacteria-archaea network. The CH_4 production potential and pathways were further evaluated through dynamic, thermodynamic and ^{13}C stable isotope analysis. The powerful CH_4 production potential benefited from the metabolic flux: classical polysaccharides, soluble sugar (glucose, galactose, lactose), acetate, and CH_4 produced via typical acetoclastic methanogenesis. In comparison, a cooperative model dominated by hydrogenotrophic methanogenic archaea presented a weak ability to generate CH_4. Our findings comprehensively link carbon and CH_4 metabolism paradigm to specific microbial lineages which are shaped related to developmental stages of the dairy cattle, directing influencing global warming from livestock and waste treatment.

Keywords: Cow feces; Biomethane; Metagenome-assembled genome; Network analysis

1. Introduction

Climate warming is a global problem of great concern but difficult to contain. In

a global context, farm animals exacerbate greenhouse gas emissions via ruminants, manure, and land use to meet increasing global food demand (Boetius, 2019). Livestock has became the second-largest anthropogenic contributor to the global CH_4 budget, contributing to nearly one-fifth of total emissions (Chang et al., 2019; Mizrahi et al., 2021; Saunois et al., 2016). Based on data from the Food and Agriculture Organization (FAO) on CH_4 emission in 2019, India, Brazil, China, and the United States of America are the top four CH_4 emitters, each exceeding 6 Tg/a (Fig. S1a). Cattle (non-dairy and dairy), buffaloes, goats, and sheep are recognized as the main livestock types, together representing 96% of the global enteric fermentation source for CH_4 emission, with a total of more than 100 Tg in 2019 (Fig. S1).

Livestock waste is considered an important breeding ground for CH_4 production (Hou et al., 2017; Owen and Silver, 2015). Steady attention on CH_4 emission from biowaste of livestock is proposed, suggesting its deterioration on the global climate (Bhattacharya et al., 1997; Hou et al., 2015). Most developing regions, such as Asia, Latin America, and Africa, have experienced a significant increase in emissions since 1961 (Dangal et al., 2017). Studies also highlight the geographical distribution and temporal variations of CH_4 emissions from ruminants (Chang et al., 2019; Perez-Barberia, 2017). Given that the recent Intergovernmental Panel on Climate Change (IPCC) report on the 'Impacts of 1.5 °C of Global Warming on Natural and Human Systems' provides evidence for the urgency of our short-term future plans (IPCC, 2022), only a tiny amount of atmospheric carbon credits remain before we reach the irreversible tipping point.

Recently, a Bayesian modeling analysis discovered that rumen microbiota influence dairy cattle CH_4 emission (Zhang et al., 2020). Specific enrichment of microbes and metabolic pathways was proposed to improve energy and carbon

channeling, acccompanied by a decrease in CH_4 emission into the atmosphere (Kruger et al., 2016). It is widely accepted that the production of CH_4 mainly comes from the function and metabolism of archaea. However, Metagenome and metatranscriptome analyses of the rumen in low CH_4-yielding sheep revealed lactic acid formation and utilization controlled by bacteria (Kamke et al., 2016), despite host-archaeal community interactions suggesting substantial CH_4 production (Borrel et al., 2020). Anaerobic fungi can also outcompete bacteria and archaea, playing a significant role in CH_4 release during polysaccharide degradation (Peng, 2021). These results provoke key fundamental questions: what are the drivers of the large CH_4 emissions from livestock waste, and are they related to microbial syntrophy processes, including changes in microbial community composition, diversity, activity, and developmental stages of host?

In this study, we analyzed whether and how methanogenic archaea form stable association with bacteria in diverse dairy cattle wastes from different developmental stages. Based on experimental results from kinetic analysis, stable isotope analysis, and metagenome-assembled genomes (MAGs), we hypothesized that a microbiota-first strategy, rather than a single-flora approach, restricts methanogenic strategies and their greenhouse effects.

2. Material and methods

2.1. Sample collection and cultivation experiments

Dairy cattle feces samples from different developmental stages were acquired at the Hebei Adopt A Dairy cattle^{TM} Dairy Co. Ltd. The facility was environmentally controlled and maintained high hygiene standards . All dairy cattle were fed a similar standard corn–soy diet with a minimum metabolizable energy of ~ 3,200 kcal/kg. The diet of 1-year(yr)-old group contained a lower proportion of silage corn (~70 %), which

is ~80 % and >90 % for the group of 1.5- and 2.5/4-yr-old groups. Fresh rectal feces were collected from each group with at least 3 replicates.

For the cultivation experiments, 1 g fresh feces and 5 g of water were added to serum bottles. Vacuum/charging high-purity nitrogen (3 cycles) were conducted to establish an anaerobic environment. The bottles were kept at 30 ℃ in the dark for 22 days. Serum bottles were sacrificed in triplicate to test CH_4 and CO_2 concentrations. Tests for pH and acetate concentration was also performed. Stable isotope analysis was conducted on samples collected on day 22.

2.2. Chemical analysis

A gas chromatography (GC; Agilent 7820A, USA) equipped with a flame ionization detector (FID) was used to analyse biogas concentrations. Acetate concentration was measured using a high-performance liquid chromatography (HPLC) apparatus (Agilent 1260 Infinity) equipped with a refractive index detector (RID) referring to previous studies (Xiao et al., 2019).

2.3. Carbon Stable Isotope Analysis

Carbon stable isotopes was measured using a gas chromatograph combustion isotope ratio mass spectrometer (GC–C–IRMS) system (Thermo Fisher MAT253, Germany). CH_4 and CO_2 were firstly separated by a Finnigan Precon. The separated CH_4 was injected into a 100 ml container prefilled with helium gas. The mixture was loaded into a chemical trap which can remove CO_2 and H_2O. Then, CH_4 can be oxidized to CO_2 and H_2O in a combustion reactor at 960 °C. The obtained CO_2 was purified by two consecutive liquid nitrogen cold traps filled with Ni wires and analysed by IRMS with a precision of ±0.2‰ for 1.3 nmol CH_4. The δ notation was used to denote the abundance of ^{13}C as follows (Xiao et al., 2019; Gehring et al., 2015):

$$\delta^{13}C = \left[\frac{\left(\frac{^{13}C}{^{12}C}\right)_{sample}}{\left(\frac{^{13}C}{^{12}C}\right)_{PDB}} - 1\right] \times 1000$$

where the standard is from Pee Dee Belemnite (PDB) carbonate with a $^{13}C/^{12}C$ ratio of 0.0112372. The measurement of $\delta^{13}C$-values of CO_2 was similar, where a water trap was used to replace the chemical trap. The α value can be calculated using the following equation (Xiao et al., 2019; Gehring et al., 2015):

$$\alpha = \frac{\delta^{13}CO_2 + 1000}{\delta^{13}CH_4 + 1000}$$

2.4. Calculation of Gibbs free energy for acetoclastic methanogenesis

For the calculation of ΔG of acetoclastic methanogenesis, the following equation is used:

$$\Delta G = \Delta G^0 + RT * \left\{\ln\left[\frac{C_{CH_4} * C_{CO_2}}{(C_{acetate})}\right]\right\} + 2.303 * RT * N_{pH}$$

where ΔG^0, ΔG are the Gibbs free energy at 273.15 K and 101.325 kPa; R is the ideal gas constant, 8.3145 J·mol^{-1}·K^{-1}; T is the absolute thermodynamic temperature, 303.15 K; C_{CH_4}, C_{CO_2} and C_{H_2} represent the concentrations of CH_4, CO_2, and H_2 in mol·L^{-1}. For the calculation of ΔG^0, use $\Delta G^0=\Delta G_f^0 - \Delta S*(T_f-T_0)$, where ΔG_f^0 is the Gibbs free energy under 298.15 K and 101.325 kPa; ΔS is the entropy change at 298.15 K; T_f and T_0 are 298.15 K and 273.15 K, respectively. ΔG_f^0 is calculated as $\Delta G_f^0=\Delta H - T_f*\Delta S$, where ΔH is the enthalpy change at 298.15 K. $C_{acetate}$ is the acetate concentration in mol·L^{-1} and N_{pH} is the pH value of the supernatant.

2.5. DNA extraction, separation, and sequencing

The samples at day 22 were collected for metagenomic sequencing. To verify the generalizability of the data, we collected dairy cattle samples from another city, Beijing Sanyuan Food Co. Ltd. (ShouGuang, China), for microbiome analysis. The E.Z.N.A.®

Soil DNA Kit made by Omega Bio-tek, Norcross, GA, U.S. was used to extract the total DNA. The NEXTflex^{TM} Rapid DNA-Seq Kit (Bio Scientific, Austin, TX, USA) was used to construct paired-end libraries. Adapters containing the full complement of sequencing primer hybridization sites were ligated to the blunt end of the fragments. The libraries were sequenced using Illumina Hiseq Xten technology (Illumina Inc., San Diego, CA, USA) at OEBiotech Co., Ltd. (Qingdao, China) using HiSeq X Reagent Kits according to the instructions from the manufacturer for 150 bp paired-end sequences. Sequence data associated with this project was deposited in the National Microbiology Data Center (Beijing, China) with under accession number NMDC10018086.

2.6. Assembly of metagenomic data sets

A Linux server equipped with 88 CPU cores and 1T RAM was used to conduct the *de novo* assembly of the metagenomic sequences. Trimmomatic was used to remove adapters and filter low quality reads (Bolger et al., 2014). Contaminations were removed by aligning our reads to the human genome Hg38 using BBmap. The final clean reads from all eight samples were co-assembled using MEGAHIT with default parameters (Li et al., 2015). Finally, only contigs larger than 500 bp were selected for downstream analysis. QUAST was used to assess the quality of the assembly (Gurevich et al., 2013).

2.7. Genomic binning and annotation

The binning process was performed with MetaWRAP (Uritskiv et al., 2018). Briefly, the assembly was binned with MaxBin2 (Wu et al., 2016), MetaBAT2 (Kang et al., 2019), and CONCOCT (Alneberg et al., 2014) with the binning module, respectively. The produced MAGs were refined using the bin_refinment module with completeness > 50%, contamination < 10% as thresholds. The filtered MAGs were

179 further improved using the bin_reassembly module, which reassemble the MAGs with
180 SPAdes (Bankevich et al., 2012). The bin_quant module was used to quantify the final
181 MAGs (Patro et al., 2017), and calculate the average counts for each MAG. Then each
182 MAG was normalized as copies per million reads.

183 Taxonomy annotation of the MAGs was carried out using the Genome Taxonomy
184 Database Toolkit (GTDB-Tk, Chaumeil et al., 2020). It first predicted the ORFs of the
185 MAGs using Prodigal (Hyatt et al., 2010), then 120 single copy genes for bacteria and
186 122 single copy genes for archaea were retrieved and aligned using the GTDB database.
187 The concatenated alignment was then used to build a phylogenetic tree. Meanwhile the
188 average nucleotide identity (ANI) of the MAGs was calculated using FastANI (Jain et
189 al., 2018). The taxonomy annotation was performed based on their position in the
190 phylogenetic tree and the ANI similarity.

191 The ORFs in the MAGs were predicted using Prodigal (Hyatt et al., 2010) with
192 default parameters. EggNOG-Mapper was used to annotate the final protein sequence
193 files (Huerta-Cepas et al., 2017), aligning the protein sequences to the pre-built database
194 and annotating their function, KEGG assignment, GO assignment, and COG
195 assignment by the best hit. Carbohydrate-active enzymes (CAZys) were identified
196 using dbCAN2 with the CAZy database (Zhang et al., 2018). The R package Vegan was
197 used to perform PCoA analysis of Bray-Curtis distance based on KEGG and CAZy
198 abundances.

199 The encoding of whole carbon metabolism pathways was inferred from genomes
200 using KEGG modules, including both those available from KEGG and several custom
201 modules (Table S1, Woodcroft et al., 2018). Pathway abundance was calculated as the
202 average abundance of the individual steps within each pathway.

203 **2.8. Phylogenetic analysis**

The genomes were subjected to GTDB-Tk (Chaumeil et al., 2020) to align the single copy genes as described above. Then the concatenated alignments were used to build the phylogenetic tree using IQtree with 100 times bootstrap (Nguyen et al., 2014).

2.9. Composition analysis

We assessed the microbial composition at reads level using Kraken2 (Wood et al., 2019). With Kraken2, the reads were aligned with the RefSeq database, and the taxonomy assignments were selected through the LZW ancestor algorithm. The alpha diversity was calculated at species levels with the Microbiome package in R (www.r-project.org). Vegan was used to perform PCoA analysis of Bray-Curtis distance based on species count.

2.10. Bi-partite Co-occurrence network analysis

CoNet was used to construct the co-occurrence network of MAGs (with average abundance > 1 copy per million reads and presented in at least two-thirds of the samples) using an ensemble approach combined with the ReBoot technique. Downstream analysis only considered the edges with FDR < 0.05. Edge classified as "mutual exclusion" and "co-presence" represented negative (e.g., competitive) and positive (e.g., cooperative) relationship between pairs of MAGs, respectively. The bacteria-methanogen bi-partite network was generated by selecting connections between bacterial MAGs and methanogen MAGs.

2.11. Correlation analysis

The Pearson's correlation coefficient was calculated by the corAndPvalue function using the R package WGCNA (Langfelder and Horvath, 2008). The corresponding p values were adjusted by the Benjamini & Hochberg method through the R package multtest. The adjusted p value < 0.05 was considered statistically significant.

2.12. Statistical analysis

The comparison of the abundance of MAGs in different groups was calculated using R package limma. Only MAGs with adjusted $p < 0.05$ and $\log_2$ (fold change) > 1 or < -1 for all three comparisons were considered as significantly different MAGs.

3. Results

3.1. CH_4 production potential and pathways

Dairy cattle wastes used in this study (from four developmental stages: 1-, 1.5-, 2.5- and 4-year(yr)-old) showed distinct CH_4-producing potential (Fig. 1a). At the developmental stage (approximately 1-yr-old), it outcompeted other groups with a maximum CH_4 potential of 30 mM. The intermediate stage (2.5-yr-old) showed a significant decrease to 8 mM compared to the developmental stage ($p = 0.023$). The oldest group (4-yr-old) showed the lowest CH_4 potential (~5 mM) (Fig. 1a). Acetate concentration increased to 20 mM and then reduced to less than 3 mM for 1-yr-old group (Fig. 1b), demonstrating a positive production-consumption relationship with CH_4. Stable isotope analysis demonstrated that $\delta^{13}C$-CH_4 (Fig. S2) and the α-value (Fig. 1c) at the early stage were -40‰ and 1.025, respectively, falling within the range of typical acetoclastic methanogenesis. On the other hand, the oldest group showed a large proportion of CO_2 reduction to generate CH_4 with values of -60‰ and 1.05 for $\delta^{13}C$-CH_4 and the α-value, respectively. Feces from middle developmental stages appeared to produce CH_4 via both pathways (-50‰ and 1.04 for the 1.5-yr-old group, -45‰ and 1.03 for the 2.5-yr-old group, Fig. 1c). The Gibbs free energy of acetoclastic methanogenesis for the feces of 1-yr-old group increased slightly over the last days of the experiment, but remained below -20 $kJ \cdot mol^{-1}$ (Fig. 1d). The Gibbs free energy for the other groups was under -40 $kJ \cdot mol^{-1}$ and varied scarcely during the cultivation

period.

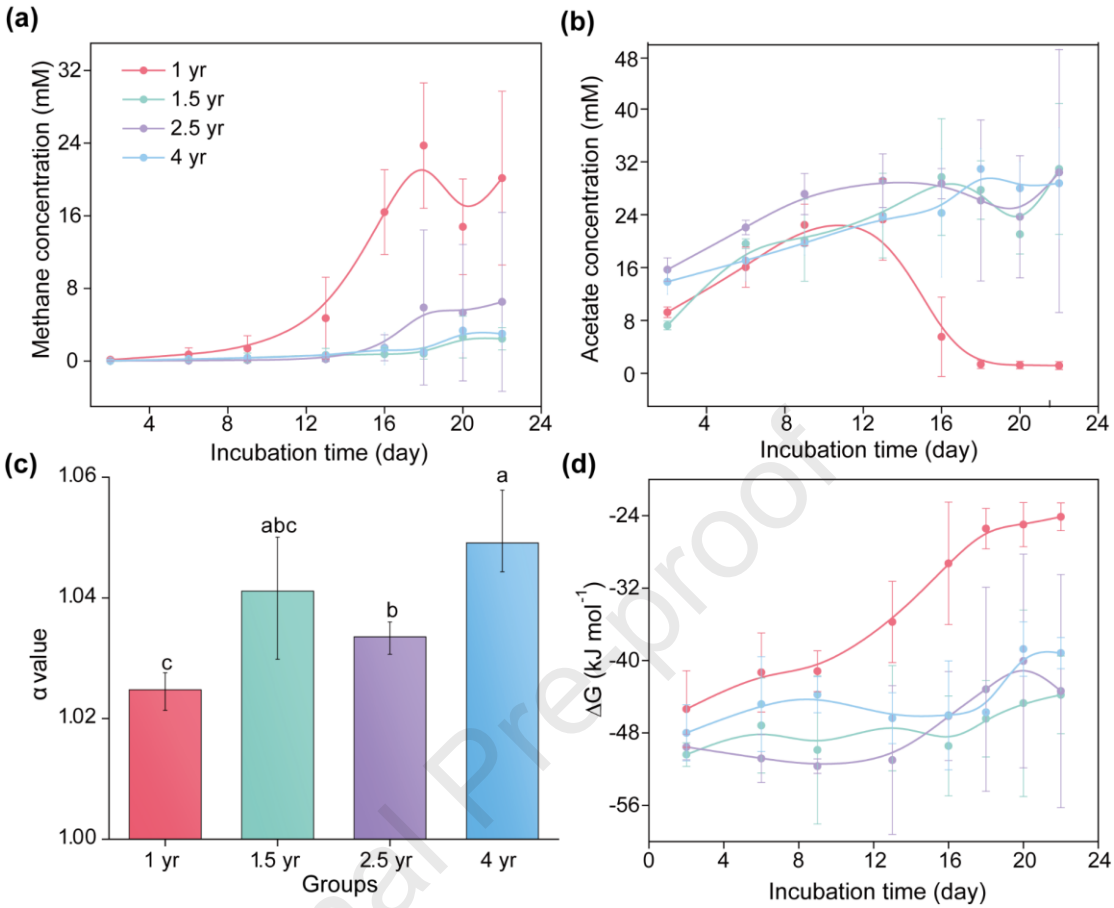

Fig. 1. CH_4 production strategies of dairy cattle feces. (a) CH_4 concentration; (b) acetate concentration; (c) α-value; (d) Gibbs free energy of acetoclastic methanogenesis dynamics.

3.2. Recovery and distribution of MAGs

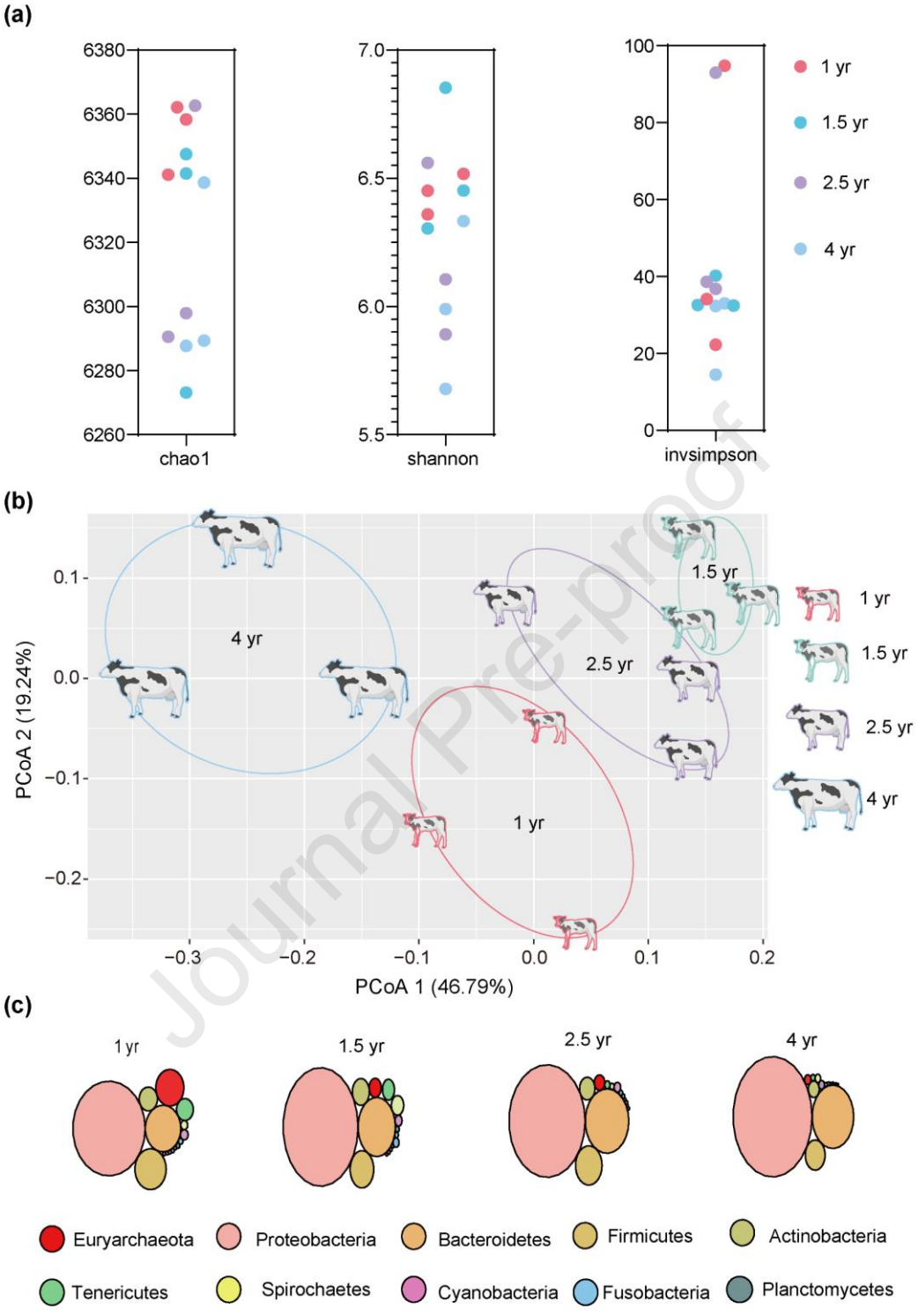

Fig. 2 The reads composition of the fecal microbiome for distinct dairy cattle. (a) α diversities at reads level of the gut microbiome; (b) PCoA analysis based on the Bray-Curtis distance of the samples; (c) The composition at the phylum level of the

gut microbiome. Note: The size of the dairy cattle diagram in (b) only represents the difference in developmental stages, not their body size.

We obtained over 120 Gbp of high-quality metagenome sequencing data. The high-quality reads obtained were also co-assembled, resulting in 304,847 contigs with an N50 of 8,288 bp. A total of 288 unique bacterial (279 MAGs) and archaeal (9 MAGs) genomes were recovered through genome binning after co-assembly (Table S2), including 67 high-quality MAGs (completeness > 95% and contamination < 5%) and 221 medium quality MAGs (completeness > 50% and contamination < 10%). The overall average completeness and contamination were 82.38% and 3.71%, respectively. The recovered MAGs spanned 13 phyla, including bacteria from Firmicutes (104 MAGs), Bacteroidetes (81 MAGs), and Proteobacteria (58 MAGs), and archaea from the phylum Euryarchaeota (9 MAGs) (Fig. S3). Consistent with the heterogeneity of feces in the environment, individual MAGs with high abundance (over 1%) were found in a limited number of samples. For several genera, closely related MAGs were abundant in the feces from the four developmental stages (Table S2), reflecting a fine-scale adaptation to distinct niches in the rumen and gut.

The microbiome diversities were analyzed at the reads level, revealing no significant differences in alpha diversity indices, including Chao1, Shannon, and Inverse Simpson Index (Fig. 2a, one-way analysis of variance (ANOVA), $p > 0.05$). Microbial community structures were strongly correlated with habitat changes, as demonstrated by abundance mapping across developmental gradients (Fig. 2b, permutational multivariate analysis of variance (PERMANOVA), $p = 0.023$). At the phylum level, Proteobacteria consistently dominated (>50%), followed by Bacteroidetes (~20%) and Firmicutes (~8%) (Fig. 2c). Notably, the proportion of

289 Euryarchaeota decreased from 3% in the 1-year-old group to just 1% in the 4-year-old
290 group, dropping to the seventh most abundant component.

291 **3.3. Polysaccharide degradation**

292 The potential microbes, pathways, and interactions responsible for the degradation
293 of polymeric organic matter and CH_4 production were evaluated by examining the
294 metabolic reconstruction of the acquired MAGs (Fig. 3; Table S3). The breakdown of
295 high molecular-weight plant-derived polysaccharides was involved in the first stage,
296 primarily cellulose and hemicellulose. Cellulase- and xylanase-encoding
297 microorganisms primarily belonged to the phylum Bacteroidetes (Fig. 3, MAG
298 abundances). For cellulase-encoding microorganisms, Bacteroidetes was the most
299 abundant phylum in the feces from all four stages (31.0%, 25.9%, 36.2% and 30.4% of
300 the recovered community in the 1-, 1,5-, 2,5- and 4-yr-old group, respectively), with a
301 slight decrease in 1.5 yr-old stage. For xylanase-encoding microorganisms, the
302 abundance of Bacteroidetes was similar across all four stages (24.4%, 24.9%, 24.0%
303 and 29.0% of the recovered community in the 1-, 1,5-, 2,5- and 4-yr-old group,
304 respectively). The xylan-degrading microorganisms showed a high similarity to
305 cellulose degraders, whereas in the feces of 2.5- and 4-yr-old groups, this metabolism
306 was limited to a high number of Bacteroidetes and a smaller number of Firmicutes (Fig.
307 3). Cellulase-encoding Bacteroidetes with high relative abundances (77.1%, 56.4%,
308 86.8% and 77.0% of the recovered community in the 1-, 1,5-, 2,5- and 4-yr-old group,
309 respectively) and xylanase-encoding Bacteroidetes (70.2%, 57.7%, 88.5% and 82.9%
310 of the recovered community in the 1-, 1,5-, 2,5- and 4-yr-old group, respectively),
311 strongly suggested that the primary degraders of large polysaccharides belonged to this
312 phylum in dairy cattle feces, but polysaccharide degradation seemed not to be the key
313 factor in controlling CH_4 production.

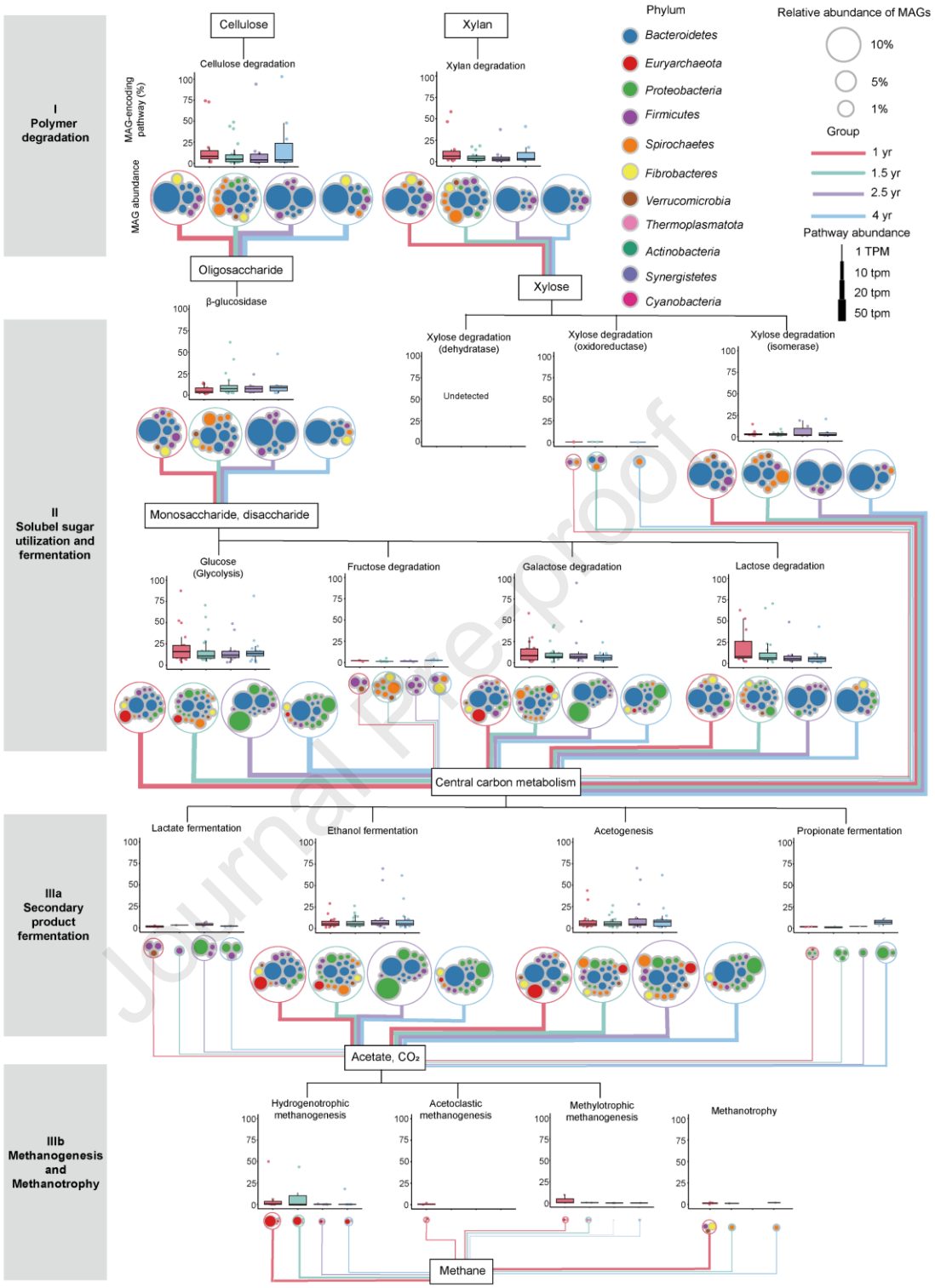

Fig. 3. Microbial carbon metabolism in feces from dairy cattle at different developmental stages. The Grey boxes in the left indicate the fermentation processes. White box plot headers and carbon compound boxes show degradation pathways. The large circles have outlines colored by group, and contain smaller circles (MAG

abundances, colored by phylum) representing the different MAGs containing genes encoding for pathways described in the scheme. Circle size indicates MAG average relative abundance. The distribution box plots are colored by group. Box plot y axes indicate the cumulative relative abundances of the MAGs containing genes encoding pathway of interest in each group, which also showed by the line thickness connecting the intermediates.

Microbial communities seek primary sources of energy and carbon by breaking down polysaccharides into simple sugars. β-Glucosidases for disaccharide degradation were encoded by microorganisms, predominantly within the Bacteroidetes phylum across all microbiomes (Fig. 3). Firmicutes were also detectable in all the samples with lower abundance, as were Fibrobacteres and Spirochaetes. Bacteroidetes was the dominant phylum, which occupies every stage of development: 1 yr-old group (81.0% of the microbial community), 1.5-yr-old group (57.5%), 2.5-yr-old group (91.4%) and 4-yr-old group (90.4%).

MAGs were also abundant in the degradation of monosaccharides such as glucose, galactose, lactose and xylose (Table S3). Fructose did not appear to be an important intermediate metabolite during polysaccharide degradation. Glucose, galactose and lactose were degraded by the same community composition (Fig. 3), but the microbial community composition varied considerably among the feces from different developmental stages of daily cattle. Glucose-degrading microorganisms showed very high similarity to those that degrade galactose. Bacteroidetes acted as the key player in monosaccharide degradation. The importance of Proteobacteria gradually manifested across developmental stages. In this case, Bacteroidetes and Proteobacteria shared a fifty-fifty basis of abundance. Interestingly, MAGs belonging to Euryarchaeota also

encoded pathways for glucose and galactose utilization, comprising 13.5% and 7.3% of the community in the early developmental stages, respectively. At later stages, glucose and galactose degradation was identified in Proteobacteria MAGs. For lactose degradation, the contribution of Bacteroidetes ran through the whole developmental stages by different Bacteroidetes classes.

The degradation pathways for monosaccharides through fermentation and acetogenesis are essential for supplying substrates for methanogenesis. Low-molecular-weight alcohols and organic acids such as ethanol, propionate, acetate, and lactate, as well as hydrogen and CO_2 can be produced during the fermentation stage. In dairy cattle feces, the microorganisms involved in ethanol metabolism overlapped almost perfectly with those involved in glucose degradation. In brief, ethanol fermentation is encoded by MAGs from the phyla Bacteroidetes and Proteobacteria (Fig. 3), which were particularly abundant in feces from older dairy cattle (72.6% and 56.8% of the community for 2.5- and 4-yr, respectively). Populations of Proteobacteria appeared to be an important propionate metabolizer (3.6%, 4.0%, 2.4% and 14.4% for 1-, 1,5-, 2,5- and 4-yr-old group, respectively). Yet, their low abundance weakened the contribution of propionate metabolism to overall CH_4 production, which also held true for lactate metabolism. Functional microorganisms involved in acidogenic metabolism were similar to those involved in glycolysis and ethanol fermentation, with a predominance of Bacteroidetes. Interestingly, a fraction of Euryarchaeota and Proteobacteria genomes were capable of acetogenesis (Fig. 3), and a contribution of this pathways was mainly limited to Euryarchaeota for the feces of the younger groups and Proteobacteria for the older group.

For methanogenesis, hydrogenotrophic methanogens basically increased in abundance from 1- to 4-yr-old groups (Fig. 3), which was not consistent with the

increase in CH_4 accumulation. Unexpectedly, Thermoplasmatota were found in all samples, suggesting there potential role in CH_4 production. Only two low-abundant acetoclastic methanogens were recovered exclusively from feces of 1-yr-old group, MAG.271 and MAG.209 (Fig. S5). Methylotrophic methanogens from Euryarchaeota and Thermoplasmatota were also recovered, but Euryarchaeota were present only in the 1-yr-old group at a low abundance (0.6%). Methanotrophs from Firmicutes, Fibrobacteres, Verrucomicrobia and Spirochaetes were also identified. Their high abundances in the feces of the 1-yr-old group suggested methanotrophs may oxidize some proportions of CH_4.

3.4. Bacteria-methanogen bi-partite co-occurrence network

We also identified 57108 genes with carbohydrate-active enzyme (CAZy) activity, belonging to 259 CAZy families (Fig. S5). Key functional microorganisms and genes were analysed and discussed (Fig. S5-S7, Table S4, S5). Bi-partite co-occurrence network analysis of bacteria-methanogen associations showed that bacteria nodes occupied a dominant proportion suggesting the importance of bacteria in the microbiomes for CH_4 production (Fig. 4a). Firmicutes and Bacteroidetes were the main contributors to this process (Fig. 4a). The four bacteria-methanogen networks with host development contained 4, 3, 2, and 1 archaeal MAGs, respectively (Fig. 4b). The number of the edges in these networks was 104, 95, 75, and 41, while the number of nodes was 68, 87, 43 and 38. Both edges and nodes gradually decreased. About 57.7% of the edges (60 out of 104) in the first group showed co-occurrence interactions. Also, about 64.2% (59 out of 95), 72% (54 out of 75), and 70.7% (29 out of 41) showed co-occurrence interactions in the other groups (Fig. 4b). Thus, the feces from daily cattle at the early stage had the strongest selectivity of bacteria-archaea association among the four stages.

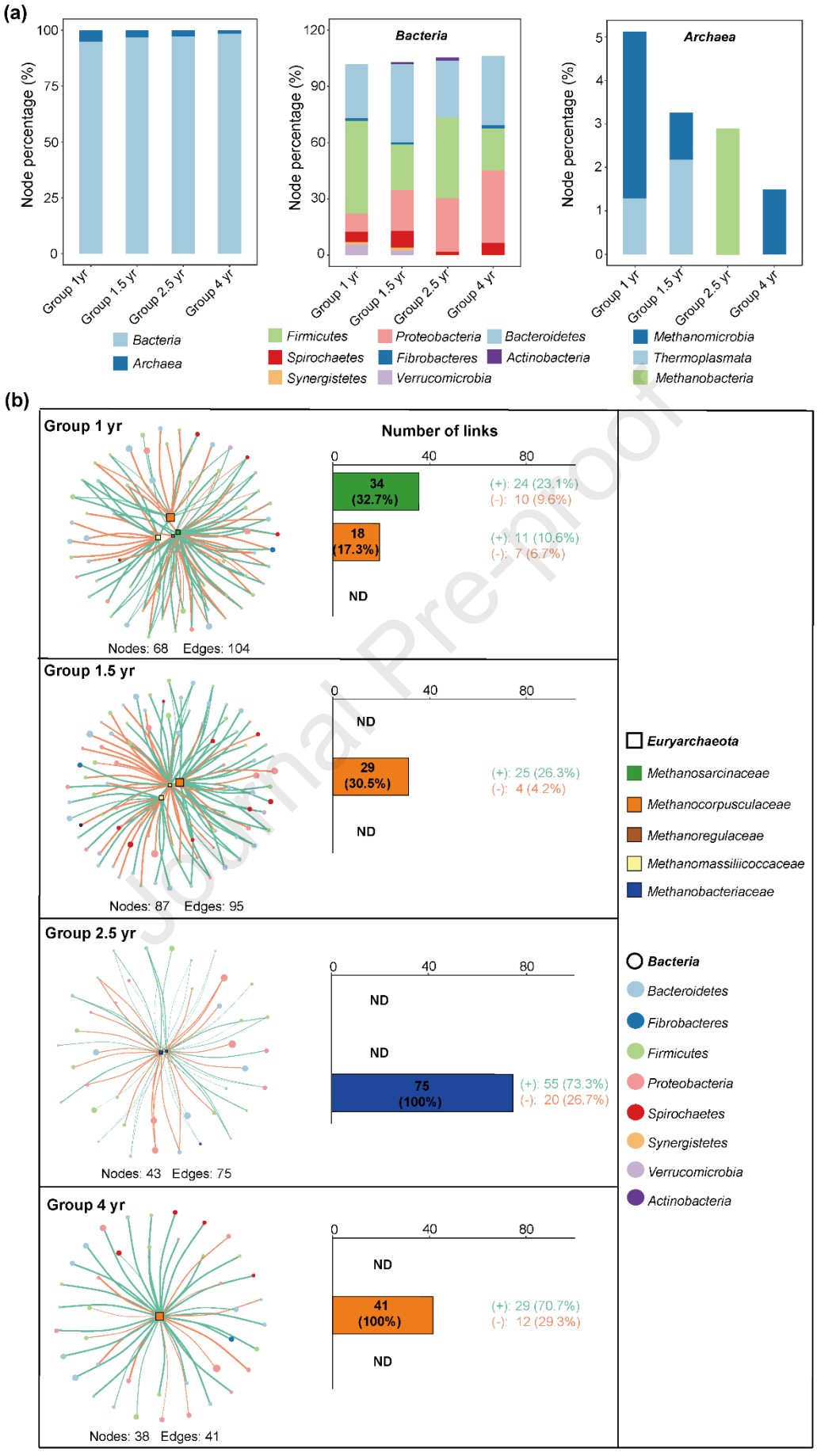
(a)
Node percentage (%)
Bacteria
Archaea
Group 1 yr
Group 1.5 yr
Group 2.5 yr
Group 4 yr
Firmicutes
Proteobacteria
Bacteroidetes
Spirochaetes
Fibrobacteres
Actinobacteria
Synergistetes
Verrucomicrobia
Methanomicrobia
Thermoplasmata
Methanobacteria
(b)
Group 1 yr
Number of links
34 (32.7%)
18 (17.3%)
ND
(+): 24 (23.1%)
(-): 10 (9.6%)
(+): 11 (10.6%)
(-): 7 (6.7%)
Nodes: 68 Edges: 104
Group 1.5 yr
29 (30.5%)
(+): 25 (26.3%)
(-): 4 (4.2%)
Nodes: 87 Edges: 95
Group 2.5 yr
75 (100%)
(+): 55 (73.3%)
(-): 20 (26.7%)
Nodes: 43 Edges: 75
Group 4 yr
41 (100%)
(+): 29 (70.7%)
(-): 12 (29.3%)
Nodes: 38 Edges: 41
Euryarchaeota
Methanosarcinaceae
Methanocorpusculaceae
Methanoregulaceae
Methanomassiliicoccaceae
Methanobacteriaceae
Bacteria
Bacteroidetes
Fibrobacteres
Firmicutes
Proteobacteria
Spirochaetes
Synergistetes
Verrucomicrobia
Actinobacteria

394

Fig. 4. Bacteria-methanogen bi-partite co-occurrence networks. (a) Node percentage of different taxonomy levels within the networks. (b) Links between bacterial MAGs and methanogen MAGs. Bar plot showed the number of links between bacterial MAGs and methanogen MAGs of *Methanosarcinaceae*, *Methanocorpusculaceae*, and *Methanobacteriaceae*. Green lines denoted co-occurrence (+). Orange lines denoted exclusion (-). Line width denoted the weight of the associations.

Archaea node percentages gradually decreased with age, suggesting a weaker co-occurrence of methanogenic archaea in later stages (Fig. 3a). MAG.271, belonging to *Methanosarcinaceae*, although at lower abundance than MAGs belonging to *Methanocorpusculaceae,* showed more connections with bacterial MAGs (34 vs 18, Fig. 3b), further confirming the crucial contribution of this low abundant methanogen. The network for feces from the 4-yr-old group contained only a hydrogenotrophic methanogen, MAG.189 (Fig. 4b), which was in accordance with the isotope analysis results showing that this group produced CH_4 mainly through CO_2 reduction.

3.5. CH_4 production affected by functional activity

Over 200 million genes were identified in the metagenomic data, belonging to 5846 KEGG gene orthologs. No noticeable differences were found among the four groups according to alpha diversities of KEGG gene orthologs (Shannon and Inverse Simpson Index, Fig. S8a, b). Nearly all genes involved in methanogenesis were positively correlated with CH_4 production (Fig. 5a). The correlation, however, was not statistically significant (p = 0.216), suggesting that methanogenic progress was potentially influenced by other factors. The PCoA analysis on the Bray-Curtis distance calculated by KEGG gene ortholog abundances showed distinct structures (Fig. S8c).

Therefore, the differences in the metabolism of microbiomes existed in the feces from diverse developmental stages.

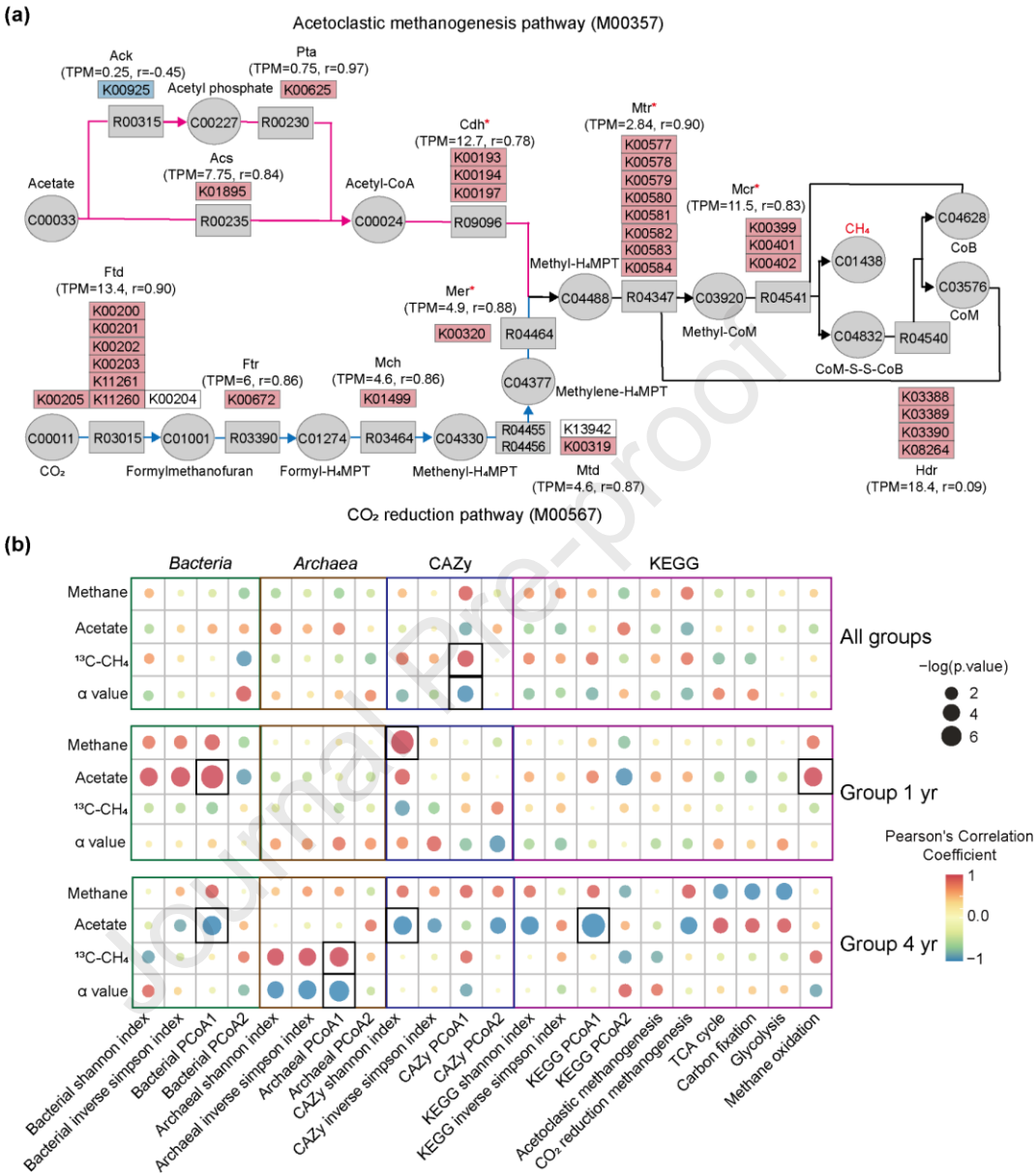

Fig. 5. Relationship between microbiome activities and CH_4 production. (a) Functional gene orthologs of methanogenesis in KEGG module M00567 and M00357. The red and blue colours indicated positive and negative correlations between KEGG gene orthologs and CH_4 production. White colours indicated undetected orthologs. Red asterisks indicated significant different orthologs ($p < 0.05$) between the 1-yr-old group and other groups. (b) Correlations between the methanogenesis parameters and the

compositional parameters at different levels. The colour of the circles indicated Pearson's correlation coefficient. The size of the circles indicated negative log10 transformed p-value. The black boxes indicated $p < 0.05$. PCoA1 and PCoA2 indicated the first and second axes during PCoA analysis baseed on Bray-Curtis distance.

By analysing all the groups together, no significant associations were observed between the compositional parameters of KEGG orthologs and CH_4 production parameters (Fig. b, *p*-values in Table S6). This may be related to the large fluctuations in microbial diversity, abundance, and function (Fig. b). The first axis (PCoA1) of CAZy families, however, was positively correlated with $\delta^{13}C\text{-}CH_4$, but negatively correlated with α-value, indicating the importance of CAZy families for methanogenic pathways. We further analyzed the key controlling factors of CH_4 production. For the early stage, bacterial PCoA1 was positively correlated with acetate production and consumption. CAZy synthesis, which are performed by bacteria, significantly affected CH_4 accumulation ($p = 0.033$), further confirmed that bacteria constrained CH_4 production.

4. Discussion

Worldwide CH_4 emissions from agricultural livestock continuously increase during the last few decades (Fig. S1b) and will expect linear growth in the future (Eshel et al., 2014). It is predicted that CH_4 generated from livestock microbiomes will reach 110 and 122 Tg by 2030 and 2050, respectively (Fig. S1b). Anthropogenic emissions (356 Tg/a) account for about two-thirds of total emissions, of which livestock accounts for 100–117 Tg/a, emanating either from the biowaste generated by farms, such as feces and/or manure, or directly by exhalation (Maasakkers et al., 2019). As shown in Fig.

S1c, high dairy cattle stocking (265 million in 2019) and ruminant behavior results in CH_4 releases accounting for about one-quarter of the total livestock. Feces and manure microbiomes are receiving increasing attention in managing CH_4 emissions (Difford et al., 2018; Wallace et al., 2019).

In general, the abundance of methanogens is correlated to high methane emissions, whereas no other direct correlations have been reported (Kruger et al., 2016; Zhou et al., 2009). These inconsistencies lie in the lack of clarity on the key microbiomes for CH_4 production. As reported, the genus *Methanobrevibacter* (*Methanobacteriales* order) is dominant, accounting for up to 70% of the rumen archaeal community (Borrel et al., 2020; Friedman et al., 2017). However, *Methanobrevibacter* seemed not to be a crucial methanogenic archaeon in this study, especially in the feces from the early developmental stage, where they were found to be only 0.017% abundance (Fig. S5). Our results also revealed that archaea with the ability to produce CH_4 were also found in the phylum Thermoplasmatota, suggesting diverse linkages of methanogenic archaea (Fig. 3, Table S3). Methanogen is not the only factor determining CH_4 production potential (Fig. 1, 3), and the relationship between CH_4 production and microbiome structure remains largely uncertain. However, the variation in composition of the core bacteria and archaea was successfully used to predict the amounts of CH_4 emissions with high accuracy (Evans et al., 2015) (Fig. S9, Table S7). Low-abundance taxa, such as *Methanosarcina*, showed close associations with predominant members (Fig. 4, S5). The microbial web of interactions in the microbiome defined the ultimate community composition, function and, thus, outcome (CH_4 production) (Fig. 1, 4, 5). In the different developmental stages studied in the present study, the rumen ecosystem was stabilized at several alternative microbiome states depending on the microbial interaction types and the strength of the resulting metabolic feedback (Fig. 3, 3), agreed

with previous study (Vanwonterghem et al., 2016). Despite the initial species pool showing a long-lasting effect on the assembly process and adult composition of the feces microbiome (Poulsen et al., 2013), there were substantial differences in the functional microbial abundance with temporal change (Fig. S5).

We categorized microorganisms using similar input and output metabolites into functional groups guiding assemblies. All metabolic cascades of the feces from distinct developmental stages were carried out by the microbial community in a complex and coordinated manner, whereby successive cross-feeding across food webs existed among a diverse collection of microbes (Fig. 3). Kamke et al. (2016) found a high hydrogenotrophic methanogenic gene expression of sheep gastrointestinal tract. Similarly, the hydrogenotrophic methanogen, *Methanobrevibacter* was more active in ruminants with strong CH_4 production (Sasson et al., 2017). It was suggested that methanogenic archaea, and in particular *Methanobrevibacter* species, are extraordinarily well-adapted to interact with animal hosts and non-archaeal components of their microbiomes (Borrel et al., 2020). As our findings in the 2.5-yr-old group, *Methanobrevibacter* was indeed the most abundant, 14.6 times more abundant than the other groups combined. It is worth noting that a higher proportion of Euryarchaeota in the 1-yr-old group relative to the 2.5-year-old group was observed, implying that other Euryarchaeota taxa may be more prominent in the 1-yr-old group, contributing to the overall higher concentration of Euryarchaeota. Besides, the benefit from CAZys encoding for degradation of pectate and oligogalacturonate with an increased trend in the feces from later developmental stages, such as PL-10, GH138, and GH 139 (Fig. S4c), suggests the improvement of macromolecular carbon utilization efficiency. Due to the predominance of hydrogenotrophic methanogenesis by *Methanobrevibacter*, there was a high probability that the metabolic flow proceeds in the following order:

polysaccharides, soluble sugar (glucose, galactose, lactose), H_2 and CO_2, CH_4.

Extreme high biogas accumulation, however, was found in the feces from the early developmental stage and speculated that metabolic cascades contribute to polysaccharide degradation. Carbohydrate-active enzymes preferred classical polysaccharides (Fig. S5c). Soluble sugar utilization to central carbon metabolism is a crucial pathway which can provide sufficient substrates, such as acetate, for subsequent metabolism (Morais and Mizrahi, 2019). The establishment of a robust stable community, mainly from Bacteroidetes and Euryarchaeota, is connected to CH_4 emission. The isotope evidence confirmed that CH_4 was reliably derived from the direct disproportionation cracking of acetate (Fig. 1, S2). Therefore, its unique acetoclastic methanogenesis pathway was also the guarantee of high CH_4 production (Furman et al., 2020; Greening et al., 2019). Isotope analysis also confirmed that acetoclastic methanogenesis was prevalent in diverse anaerobic systems (Greening et al., 2019; Han et al., 2017; Xiao et al., 2020a; Xiao et al., 2020b; Li et al., 2018), which were previously believed to be dominated by CO_2 reduction pathway (Yu et al., 2022; Park et al; Xiao et al., 2018). The prevalence of direct interspecies electron transfer (DIET) in the past decade may cover the inherent methanogenic strategy (Morita et al., 2011; Rotaru et al., 2014; Wegener et al., 2015). In this study, the analysis of electroactive microorganisms revealed that these bacteria were in very low abundance (Fig. 2, Fig. S6). The negative correlation of these microbial abundances with CH_4 production potential denied this possibility of CH_4 from electron reduction of CO_2.

Network analysis clearly supported a microbiota-first strategy, with targeted corporation driving enhanced CH_4 emission (Fig. 3). In there, the low abundance of *Methanosarcinaceae* outcompeted the high abundance of *Methanocorpusculaceae*, involving a large number of nodes and edges, and evenly distributed multiple

interaction types (Fig. 3b). Stoichiometric results (acetate consumption and CH_4 production) also showed a perfect match via acetoclastic pathway rather than CO_2 reduction (Fig. 1), as our previous study evidenced (Xiao et al., 2020a). Thus, in the 1-year-old group, the acetoclastic methanogens (*Methanosarcinaceae*, MAG.271) and related bacteria formed a targeted cooperative network for methane production through acetate dissimilation. Similarly, in the 4-year-old group, Methanocorpusculaceae (MAG.189) formed a targeted cooperation for CO2 reduction. Combined microbiomes, rather than individual methanogens even with the highest abundance, controlled methane-producing potential. For Gibbs free energy of acetoclastic methanogenesis, this pathway was always thermodynamically feasible (Fig. 1d). The major metabolic flux for powerful CH_4 production in the feces from the early developmental stage holds polysaccharides, soluble sugar (glucose, galactose, lactose), acetate and CH_4. Nevertheless, open questions also include what the precise functions are in the highly abundant methanogens.

5. Conclusion

This study proved almost 6 times higher CH_4 production of young dairy cattle manure compared to older ones. Metagenomic assembled genomes analysis revealed the methane producing metabolic flux. Powerful CH_4 production potential was achieved via typical acetoclastic methanogenesis, which is validated through stable isotope and network analysis. However, a cooperative model dominated by hydrogenotrophic methanogenic archaea presented weak CH_4 production. Our findings comprehensively link carbon and CH_4 metabolism paradigms to specific microbial lineages, which are shaped by the developmental stages of dairy cattle. In conclusion, the interplay between microbial community composition, metabolic pathways, and microbial interactions plays a crucial role in the higher CH_4 production observed in

young dairy cattle manure. Specifically, the dominance of acetoclastic methanogens, the higher proportion of Euryarchaeota taxa, the close interactions between bacteria and methanogens, and the presence of carbohydrate-active enzymes all contribute to the enhanced methane production in younger cattle manure. These factors emphasize the significant influence of microbial dynamics and metabolic processes on CH_4 output.

Declaration of Competing Interest

The authors declare that they have no known competing financial interests or personal relationships that could have appeared to influence the work reported in this paper.

Data and materials availability

All data needed to evaluate the conclusions in the paper are present in the paper and/or the Supplementary Materials. The metagenomic sequencing data have been deposited in the National Microbiology Data Center with an accession number NMDC10018086.

Funding

This work was supported by the Natural Science Foundation of Heilongjiang Province in China (YQ2023D007), the Youth Innovation Promotion Association of CAS (2021213), the National Natural Science Foundation of China (42307437, 42077025, 42277236), the Youth Science and Technology Innovation Plan of Universities in Shandong (2019KJE007), and Research Project of Dezhou University (2023XKZX004). M.H. gratefully acknowledges Royal Society Dorothy Hodgkin Research Fellowship (DHF\R1\211076).

CRediT authorship contribution statement

Jian Liu: Methodology, Investigation, Visualization, Writing—original draft, Writing—review & editing. **Meng Zhou:** Visualization, Investigation, Writing—review & editing. **Lifeng Zhou:** Methodology. **Run Dang:** Investigation. **Leilei Xiao:** Conceptualization, Methodology, Investigation, Visualization, Writing—original draft, Writing—review & editing. **Yang Tan:** Methodology. **Meng Li:** Investigation. **Jiafeng Yu:** Methodology, Investigation, Visualization, Supervision, Writing—original draft. **Peng Zhang:** Visualization. **Marcela Hernández:** Methodology, Writing—original draft, Writing—review & editing. **Eric Lichtfouse:** Investigation, Writing—original draft, Writing—review & editing.

References

Alneberg, J., Bjarnason, B.S., de Bruijn, I., Schirmer, M., Quick, J., Ijaz, U.Z., Lahti, L., Loman, N.J., Andersson, A.F., Quince, C., 2014. Binning metagenomic contigs by coverage and composition. Nat. Methods. 11, 1144–1146. https://doi.org/10.1038/nmeth.3103.

Bankevich, A., Nurk, S., Antipov, D., Gurevich, A.A., Dvorkin, M., Kulikov, A.S., Lesin, V.M., Nikolenko, S.I., Pham, S.K., Prjibelski, A.D., Pyshkin, A., Sirotkin, A., Vyahhi, N., Tesler, G., Alekseyev, M.A., Pevzner, P.A., 2012. SPAdes: A new genome assembly algorithm and its applications to single-cell sequencing. J. Comput. Biol. 19, 455–477. https://doi.org/10.1089/cmb.2012.0021.

Bhattacharya, S.C., Thomas, J.M., Salam, P.A., 1997. Greenhouse gas emissions and the mitigation potential of using animal wastes in Asia. Energy 22, 1079–1085. https://doi.org/10.1016/S0360-5442(97)00039-X.

Boetius, A., 2019. Global change microbiology — big questions about small life for our future. Nat. Rev. Microbiol. 17, 331–332. https://doi.org/10.1038/s41579-019-0197-2.

Bolger. A.M., Lohse. M. Usadel, B., 2014. Trimmomatic: A flexible trimmer for Illumina sequence data. Bioinformatics 30, 2114–2120. https://doi.org/10.1093/bioinformatics/btu170.

Borrel, G., Brugère, J.F., Gribaldo, S., Schmitz, R.A., Moissl-Eichinger C. 2020. The host-associated archaeome. Nat. Rev. Microbiol. 18, 622–636. https://doi.org/10.1038/s41579-020-0407-y.

Chadwick, D., Sommer, S., Thorman, R., Fangueiro, L., Cardenas, L., Amon, B., Misselbrook, T., 2011. Manure management: Implications for greenhouse gas emissions. Anim. Feed Sci. Technol. 166–167, 514–531. https://doi.org/10.1016/j.anifeedsci.2011.04.036

Chang, J.f., Peng, S.S., Ciais, P., Saunois, M., Dangal, S.R.S., Herrero, M., Havlik, P., Tian, H.Q., Bousquet, P., 2019. Revisiting enteric methane emissions from domestic ruminants and their $\delta^{13}CCH_4$ source signature. Nat. Commun. 10, 2441-1723 3420. https://doi.org/10.1038/s41467-019-11066-3.

Chaumeil, P. A., Mussig, A. J., Hugenholtz, P. Parks, D. H., 2020. GTDB-Tk: A toolkit to classify genomes with the genome taxonomy database. Bioinformatics 36, 1925–1927. https://doi.org/10.1093/bioinformatics/btz848.

Dangal, S.R.S., Tian, H., Zhang, B., Pan, S.F., Lu, C.Q., Yang, J., 2017. Methane emission from global livestock sector during 1890-2014: Magnitude, trends and spatiotemporal patterns. Glob. Chang Biol. 23, 4147–4161. https://doi.org/10.1111/gcb.13709.

628 Difford, G.F., Plichta, D.R., Løvendahl, P., Lassen, J., Noel, S.J., Højberg, O., Wright
629 A.G., Zhu, Z., Kristensen, L., Nielsen, H.B., Guldbrandtsen, B., Sahana, G.. 2018.
630 Host genetics and the rumen microbiome jointly associate with methane emissions
631 in dairy cows. PLos. Genet. 14, e1007580.
632 https://doi.org/10.1371/journal.pgen.1007580.
633 Eshel, G., Shepon, A., Makov, T., Milo, R., 2014. Land, irrigation water, greenhouse
634 gas, and reactive nitrogen burdens of meat, eggs, and dairy production in the
635 United States. Proc. Natl. Acad. Sci. USA. 111, 11996–12001.
636 https://doi.org/10.1073/pnas.1402183111.
637 Evans, P.N., Parks, D.H., Chadwick, G.L., Robbins, S.J., Orphan, V.J., Golding, S.D.,
638 Tyson, G.W., 2015. Methane metabolism in the archaeal phylum Bathyarchaeota
639 revealed by genome-centric metagenomics. Science 350, 434–438.
640 https://doi.org/10.1126/science.aac7745.
641 Friedman, N., Shriker, E., Gold, B.S., Durman, T., Zarecki, R., Ruppin, E., Mizrahi, I.,
642 2017. Diet-induced changes of redox potential underlie compositional shifts in the
643 rumen archaeal community. Environ. Microbiol. 19, 174–184.
644 https://doi.org/10.1111/1462-2920.13551.
645 Furman, O., Shenhav, L., Sasson, G., Kokou, F., Honig, H., Jacoby, S., Hertz, T.,
646 Cordero, O.X., Halperin, E., Mizrahi, I., 2020. Stochasticity constrained by
647 deterministic effects of diet and age drive rumen microbiome assembly dynamics.
648 PLoS. Comput. Biol. 13, e1005404. https://doi.org/10.1038/s41467-020-15652-8.
649 Gehring, T.A., Klang, J., Niedermayr, A., Berzio, S., Immenhauser, A., Klocke, M.,
650 Wichern, M., Lübken, M., 2015. Determination of methanogenic pathways
651 through carbon isotope ($\delta^{13}C$) analysis for the two-stage anaerobic digestion of

652 high-solids substrates. Environ. Sci. Technol. 49, 4705–4714.
653 https://doi.org/10.1021/es505665z.
654 Greening, C., Geier, R.R., Wang, C., Woods, L.C., Morales, S.E., McDonald, M.J.,
655 Rushton-Green, R., Morgan, X.C., Koike, S., Leahy, S.C., Kelly, W.J., Cann, I.,
656 Attwood, G.T., Cook, G.M., Mackie, R.I., 2019. Greening, C. et al. Diverse
657 hydrogen production and consumption pathways influence methane production in
658 ruminants. ISME J. 13, 2617–2632. https://doi.org/10.1038/s41396-019-0464-2.
659 Gurevich, A., Saveliev, V., Vyahhi, N., Tesler, G., 2013. QUAST: Quality assessment
660 tool for genome assemblies. Bioinformatics 29, 1072–1075.
661 https://doi.org/10.1093/bioinformatics/btt086.
662 Han, B., Duan, X., Wang, Y., Zhu, K., Zhang, J., Wang, R., Hu, H., Qi, F.J., Pan, J., Yan,
663 Y., Shen, W., 2017. Methane protects against polyethylene glycol-induced osmotic
664 stress in maize by improving sugar and ascorbic acid metabolism. Sci. Rep. 7,
665 46185. https://doi.org/10.1038/srep46185.
666 Hou, Y., Velthof, G.L., Lesschen, J.P., Staritsky, L.G., Oenama O., 2017. Nutrient
667 recovery and emissions of ammonia, nitrous oxide, and methane from animal
668 manure in Europe: Effects of manure treatment technologies. Environ. Sci.
669 Technol. 51, 375–383. https://doi.org/10.1021/acs.est.6b04524.
670 Hou, Y., Velthof, G.L., Oenema, O., 2015. Mitigation of ammonia, nitrous oxide and
671 methane emissions from manure management chains: a meta-analysis and
672 integrated assessment. Glob. Chang Biol. 21, 293–1312.
673 https://doi.org/10.1111/gcb.12767
674 Huerta-Cepas, J., Forslund, K., Coelho, L.P., Szklarczyk, D., Jensen, L.J., von Mering,
675 C., Bork, P., 2017. Fast genome-wide functional annotation through orthology

676 assignment by eggNOG-mapper. Mol. Biol. Evol. 34, 2115–2122.
677 https://doi.org/10.1101/076331.
678 Hyatt, D., Chen, G., LoCascio, P.F., Land, M.L., Larimer, F.W., Hauser, L.J., 2010.
679 Prodigal: Prokaryotic gene recognition and translation initiation site identification.
680 BMC Bioinformatics 11, 119. https://doi.org/10.1186/1471-2105-11-119.
681 IPCC., 2022. Impacts of 1.5°C Global Warming on Natural and Human Systems.
682 Global Warming of 1.5°C. 175–312. https://www.ipcc.ch/sr15/chapter/chapter-3.
683 Jain, C., Rodriguez-R, L. M., Phillippy, A. M., Konstantinidis K. T., Aluru S., 2018.
684 High throughput ANI analysis of 90K prokaryotic genomes reveals clear species
685 boundaries. Nat. Commun. 9, 5114. https://doi.org/10.1038/s41467-018-07641-9.
686 Kamke, J., Kittelmann, S., Soni, P., Li, Y., Tavendale, M., Ganesh, S., Janssen, P. H.,
687 Shi, W.B., Froula, J., Rubin, E.M., Attwood, G.T. 2016. Rumen metagenome and
688 metatranscriptome analyses of low methane yield sheep reveals a *Sharpea*-
689 enriched microbiome characterised by lactic acid formation and utilisation.
690 Microbiome 4, 56. https://doi.org/10.1186/s40168-016-0201-2.
691 Kang, D.D., Li, F., Kirton, E., Thomas, A., Egan, R., An, H., Wang, Z., 2019. MetaBAT
692 2: An adaptive binning algorithm for robust and efficient genome reconstruction
693 from metagenome assemblies. PeerJ 7, e7359. https://doi.org/10.7717/peerj.7359.
694 Kruger Ben Shabat, S., Sasson, G., Doron-Faigenboim, A., Durman, T., Yaacoby, S.,
695 Miller, M.E.B., White, B.A., Shterzer, N., Mizrahi, I., 2016. Specific microbiome-
696 dependent mechanisms underlie the energy harvest efficiency of ruminants. ISME
697 J. 10, 2958–2972. https://doi.org/10.1038/ismej.2016.62.
698 Langfelder, P., Horvath, S., 2008 WGCNA: An R package for weighted correlation
699 network analysis. BMC Bioinformatics 9, 1–13. https://doi.org/10.1186/1471-
700 2105-9-559.

Li, D., Liu, C.M., Luo, R., Sadakane, K. Lam, T., 2015. MEGAHIT: An ultra-fast single-node solution for large and complex metagenomics assembly via succinct de Bruijn graph. Bioinformatics 31, 1674–1676. https://doi.org/10.1093/bioinformatics/btv033.

Li, J., Xiao, L., Zheng, S., Zhang, Y., Luo, M., Tong, C., Xu, H., Tan, Y., Liu, J., Wang, O., Liu, F., 2018. A new insight into the strategy for methane production affected by conductive carbon cloth in wetland soil: Beneficial to acetoclastic methanogenesis instead of CO_2 reduction. Sci. Total Environ. 643, 1024–1030. https://doi.org/10.1016/j.scitotenv.2018.06.271.

Maasakkers, J.D., Jacob, D.J., Sulprizio, M.P., Scarpelli, T.R., Nesser, H., Sheng, J.X., Zhang, Y., Hersher, M., Bloom, A.A., Bowman, K.W., Worden, J.R., Janssens-Maenhout, G., Parker, R. J., 2019. Maasakkers, J. D. et al. Global distribution of methane emissions, emission trends, and OH concentrations and trends inferred from an inversion of GOSAT satellite data for 2010-2015. Atmos. Chem. Phys. 19, 7859–7881. https://doi.org/10.5194/acp-19-7859-2019.

Mizrahi, I., Wallace, R.J., Moraïs, S., 2021. The rumen microbiome: balancing food security and environmental impacts. Nat. Rev. Microbiol. 19, 553–566. https://doi.org/10.1038/s41579-021-00543-6.

Moraïs, S., Mizrahi, I., 2019. The road not taken: The rumen microbiome, functional groups, and community states. Trends Microbiol. 27, 538–549. https://doi.org/10.1016/j.tim.2018.12.011.

Morita, M., Malvankar, N.S., Franks, A.E., Summers, Z.M., Giloteaux, L., Rotaru, A., Rotaru, C., Lovley, D.R., 2011. Potential for direct interspecies electron transfer in methanogenic wastewater digester aggregates. mBio 2, e00159-11. https://doi.org/10.1128/mBio.00159-11.

726 Nguyen, L. T., Schmidt, H. A., von Haeseler, A. Minh, B. Q., 2014. IQ-TREE: A fast
727 and effective stochastic algorithm for estimating maximum-likelihood
728 phylogenies. Mol. Biol. Evol. 32, 268–274.
729 https://doi.org/10.1093/molbev/msu300.
730 Owen, J.J, Silver, W.L., 2015. Greenhouse gas emissions from dairy manure
731 management: a review of field-based studies. Glob. Chang Biol. 21, 550–565.
732 https://doi.org/10.1111/gcb.12687.
733 Park, J.H., Kang, H.J., Park, K.H., Park, H.D., 2018. Direct interspecies electron
734 transfer via conductive materials: A perspective for anaerobic digestion
735 applications. Bioresour. Technol. 254, 300–311.
736 https://doi.org/10.1016/j.biortech.2018.01.095.
737 Patro, R., Duggal, G., Love, M. I., Lrizarry, R. A. Kingsford C., 2017. Salmon provides
738 fast and bias-aware quantification of transcript expression. Nat. Methods. 14, 417–
739 419. https://doi.org/10.1038/nmeth.4197.
740 Peng, X., 2021. Genomic and functional analyses of fungal and bacterial consortia that
741 enable lignocellulose breakdown in goat gut microbiomes. Nat. Microbiol. 6, 499–
742 511. https://doi.org/10.1038/s41564-020-00861-0.
743 Pérez-Barbería, F.J., 2017. Scaling methane emissions in ruminants and global
744 estimates in wild populations. Sci. Total Environ. 579, 1572–1580.
745 https://doi.org/10.1016/j.scitotenv.2016.11.175.
746 Poulsen, M., Schwab, C., Borg Jensen, B., Engberg, R.M., Spang, A., Canibe, N.,
747 Højberg, O., Milinovich, G., Fragner, L., Schleper, C., Weckwerth, W., Lund, P.,
748 Schramm, A., Urich, T., 2013. Methylotrophic methanogenic Thermoplasmata
749 implicated in reduced methane emissions from bovine rumen. Nat. Commun. 4,
750 1428. https://doi.org/10.1038/ncomms2432.

751 Rotaru, A., Shrestha, P.M., Liu, F., Shrestha, M., Shrestha, D., Embree, M., Zengler, K.,
752 Wardman, C., Nevin, K.P., Lovley, D.R., 2014. A new model for electron flow
753 during anaerobic digestion: direct interspecies electron transfer to *Methanosaeta*
754 for the reduction of carbon dioxide to methane. Energy Environ. Sci. 7, 408–415.
755 https://doi.org/10.1039/C3EE42189A.
756 Sasson, G., Kruger Ben-Shabat, S., Seroussi, E., Doron-Faigenboim, A., Shterzer, N.,
757 Yaacoby, S., Berg Miller, M.E., White, B.A., Halperin, E., Mizrahi, I., 2017.
758 Heritable bovine rumen bacteria are phylogenetically related and correlated with
759 the cow's capacity to harvest energy from its feed. mBio 8, e00703-17.
760 https://doi.org/10.1128/mBio.00703-17.
761 Saunois, M., Bousquet, P., Poulter, B., Peregon, A., Ciais, P., Canadell, J.G.,
762 Dlugokencky, E.J., Etiope, G., Bastviken, D., Houweling, S., Janssens-Maenhout,
763 G., Tubiello, F.N., Castaldi, S., Jackson, R.B., Alexe, M., Arora, V.K., Beerling,
764 D.J., Bergamaschi, P., Blake, D.R., Brailsford, G., Brovkin, V., Bruhwiler, L.,
765 Crevoisier, C., Crill, P., Covey, K., Curry, C., Frankenberg, C., Gedney, N.,
766 Höglund-Isaksson, L., Ishizawa, M., Ito, A., Joos, F., Kim, H.-S., Kleinen, T.,
767 Krummel, P., Lamarque, J.-F., Langenfelds, R., Locatelli, R., Machida, T.,
768 Maksyutov, S., McDonald, K.C., Marshall, J., Melton, J.R., Morino, I., Naik, V.,
769 O'Doherty, S., Parmentier, F.-J. W., Patra, P.K., Peng, C., Peng, S., Peters, G. P.,
770 Pison, I., Prigent, C., Prinn, R., Ramonet, M., Riley, W.J., Saito, M., Santini, M.,
771 Schroeder, R., Simpson, I.J., Spahni, R., Steele, P., Takizawa, A., Thornton, B.F.,
772 Tian, H., Tohjima, Y., Viovy, N., Voulgarakis, A., van Weele, M., van der Werf,
773 G.R., Weiss, R., Wiedinmyer, C., Wilton, D.J., Wiltshire, A., Worthy, D., Wunch,
774 D., Xu, X., Yoshida, Y., Zhang, B., Zhang, Z., Zhu, Q., 2016 The global methane

775 budget 2000-2012. Earth Syst. Sci. Data. 8, 697–751. https://doi.org/10.5194/essd-
776 8-697-2016.
777 Uritskiy, Gv., Diruggiero, J., Taylor, J., 2018. MetaWRAP - A flexible pipeline for
778 genome-resolved metagenomic data analysis. Microbiome 6, 158.
779 https://doi.org/10.1186/s40168-018-0541-1.
780 Vanwonterghem, I., Evans, P.N., Parks, D.H., Jensen, P.D., Woodcroft, B.J., Hugenholtz,
781 P.B., Tyson, G.W., 2016. Methylotrophic methanogenesis discovered in the
782 archaeal phylum Verstraetearchaeota. Nat. Microbiol. 1, 16170.
783 https://doi.org/10.1038/NMICROBIOL.2016.170.
784 Wallace, R.J., Sasson, G., Garnsworthy, P.C., Tapio, I., Gregson, E., Bani, P., Huhtanen,
785 P., Bayat, A.R., Strozzi, F., Biscarini, F., Snelling, T.J., Saunders, N., Potterton,
786 S.L., Craigon, J., Minuti, A., Trevisi, E., Callegari, M.L., Cappelli, F.P., Cabezas-
787 Garcia, E.H., Vilkki, J., Pinares-Patiño, C.S., Fliegerová, K.O., Mrázek, J.,
788 Sechovcová, H., Kopečný, J., Bonin, A., Boyer, F., Taberlet, P., Kokou, F.,
789 Halperin, E., Williams, J.L., Shingfield, K.J., Mizrahi, I., 2019. A heritable subset
790 of the core rumen microbiome dictates dairy cow productivity and emissions. Sci.
791 Adv. 5, eaav8391. https://doi.org/10.1126/sciadv.aav8391.
792 Wegener. G., Krukenberg, V., Riedel. D., Tagetmeyer, H. E., Boetius A., 2015.
793 Intercellular wiring enables electron transfer between methanotrophic archaea and
794 bacteria. Nature 526, 587–590. https://doi.org/10.1038/nature15733.
795 Wood, D. E., Lu, J., Langmead, B., 2019. Improved metagenomic analysis with Kraken
796 2. Genome Biol. 20, 257. https://doi.org/10.1186/s13059-019-1891-0.
797 Woodcroft, B.J., Singleton, C.M., Boyd, J.A. Evans, P.N., Emerson, J.B., Zayed, A.A.F.,
798 Hoelzle, R.D., Lamberton, T.O., McCalley, C.K., Hodgkins, S.B., Wilson, R.M.,
799 Purvine, S.O., Nicora, C.D., Li, C., Frolking, S., Chanton, J.P., Crill, P.M., Saleska,

S.R., Rich, V.I., Tyson, G.W., 2018. Genome-centric view of carbon processing in thawing permafrost. Nature 560, 49–54. https://doi.org/10.1038/s41586-018-0338-1

Wu, Y-W., Simmons, B.A., Singer, S.W., 2016. MaxBin 2.0: an automated binning algorithm to recover genomes from multiple metagenomic datasets. Bioinformatics 32, 605–607. https://doi.org/10.1093/bioinformatics/btv638.

Xiao, L., Liu, F., Lichtfouse, E., Zhang, P., Feng, D., Li, F., 2020a. Methane production by acetate dismutation stimulated by *Shewanella oneidensis* and carbon materials: An alternative to classical CO_2 reduction. Chem. Eng. J. 389, e124469. https://doi.org/10.1016/j.cej.2020.124469.

Xiao, L., Liu, F., Liu, J., Li, J., Zhang, Y., Yu, J., Wang, O., 2018. Nano-Fe_3O_4 particles accelerating electromethanogenesis on an hour-long timescale in wetland soil. Environ. Sci-Nano. 5, 436–445. https://doi.org/10.1039/C7EN00577F.

Xiao, L., Sun, R., Zhang, P., Zheng, S., Tan, Y., Li, J., Zhang, Y., Liu, F., 2019. Simultaneous intensification of direct acetate cleavage and CO_2 reduction to generate methane by bioaugmentation and increased electron transfer. Chem. Eng. J. 378, 3022–3027. https://doi.org/10.1016/j.cej.2019.122229.

Xiao, L., Zheng, S., Lichtfouse, E., Luo, M., Tan, Y., Liu, F., 2020b. Carbon nanotubes accelerate acetoclastic methanogenesis: From pure cultures to anaerobic soils. Soil Biol. Biochem. 150, e107938. https://doi.org/10.1016/j.soilbio.2020.107938.

Yu J., Liu J., Senthil Kumar P., Wei Y., Zhou M., Vo D.N., Xiao L., 2022. Promotion of methane production by magnetite via increasing acetogenesis revealed by metagenome-assembled genomes. Bioresour. Technol. 345, e126521. https://www.x-mol.com/paperRedirect/1469014804960681984.

824 Zhang, H., Yohe, T., Huang, L., Entwistle, S., Wu, P., Yang, Z., Busk, P.K., Xu, Y., Yin,
825 Y., 2018. dbCAN2: a meta server for automated carbohydrate-active enzyme
826 annotation. Nucleic Acids Res. 46, W95. https://doi.org/10.1093/nar/gky418.
827 Zhang, Q.Q., Difford, G., Sahana, G., Lovendahl, P., Lassen, J., Lund, M.S.,
828 Guldbrandtden, B., Janss, L., 2020. Bayesian modeling reveals host genetics
829 associated with rumen microbiota jointly influence methane emission in dairy
830 cows. ISME J. 14, 2019–2033. https://doi.org/10.1038/s41396-020-0663-x.
831 Zhou, M., Hernandez-Sanabria, E., Le, L. G., 2009. Assessment of the microbial
832 ecology of ruminal methanogens in cattle with different feed efficiencies. Appl.
833 Environ. Microbiol. 75, 6524–6533. https://doi.org/10.1128/AEM.02815-08.

834

835 **Figure Captions**

836 **Fig. 1.** CH_4 production strategies of dairy cattle feces. (a) CH_4 concentration; (b)
837 acetate concentration; (c) α-value; (d) Gibbs free energy of acetoclastic methanogenesis
838 dynamics.

839 **Fig. 2** The reads composition of the fecal microbiome for distinct dairy cattle. (a)
840 α diversities at reads level of the gut microbiomes; (b) PCoA analysis based on the
841 Bray-Curtis distance of the samples; (c) The composition at phylum level of the gut
842 microbiomes. Note: The size of the dairy cattle diagram in (b) only represents the
843 difference in developmental stages, not their body size.

844 **Fig. 3.** Microbial carbon metabolism in feces from dairy cattle at different
845 developmental stages. The grey boxes in the left indicate the fermentation processes.
846 White box plot headers and carbon compound boxes show degradation pathways. The
847 large circles have outlines colored by group, and contain smaller circles (MAG

abundances, colored by phylum) representing the different MAGs containing genes encoding for pathways described in the scheme. Circle size indicates MAG average relative abundance. The distribution box plots are colored by group. Box plot y axes indicate the cumulative relative abundances of the MAGs containing genes encoding pathway of interest in each group, which also showed by the line thickness connecting the intermediates.

Fig. 4. Bacteria-methanogen bi-partite co-occurrence networks. (a) Node percentage of different taxonomy levels within the networks. (b) Links between bacterial MAGs and methanogen MAGs. Bar plot showed the number of links between bacterial MAGs and methanogen MAGs of *Methanosarcinaceae*, *Methanocorpusculaceae*, and *Methanobacteriaceae*. Green lines denoted co-occurrence (+). Orange lines denoted exclusion (-). Line width denoted the weight of the associations.

Fig. 5. Relationship between microbiome activities and CH_4 production. (a) Functional gene orthologs of methanogenesis in KEGG module M00567 and M00357. The red and blue colours indicated positive and negative correlations between KEGG gene orthologs and CH_4 production. White colours indicated undetected orthologs. Red asterisks indicated significant different orthologs ($p < 0.05$) between the 1-yr-old group and other groups. (b) Correlations between the methanogenesis parameters and the compositional parameters at different levels. The colour of the circles indicated the Pearson's correlation coefficient. The size of the circles indicated negative log10 transformed p-value. The black boxes indicated $p < 0.05$. PCoA1 and PCoA2 indicated the first and second axes during PCoA analysis based on Bray-Curtis distance.

Fig. S1. Global methane emissions. (a) Methane emission worldwide; (b) Methane emission in the past 40 years including the prediction for 2030 and 2060 (red dots); (c)

873 Proportion of methane emission in ruminants.

874 **Fig. S2** $\delta^{13}C$-value of CH_4 in different dairy cattle feces.

875 **Fig. S3** The number of the MAGs at phylum levels.

876 **Fig. S4** The CAZy family diversities of the microbiomes. (a) Shannon Index; (b)
877 Inverse Simpson Index; (c) The PCoA analysis of the Bray-Curtis distance based on
878 CAZy family abundances. (d) Significant different abundance of CAZy families
879 between the 1-yr-old group and other groups. The size of circles indicated the
880 abundance of CAZy families (copies per million reads). The colour of circles indicated
881 the adjusted p-values. Upper part (light yellow) indicated higher abundance in 1-yr-old
882 group. Lower part (light blue) indicated lower abundance in 1-yr-old group.

883 **Fig. S5** Exoelectrogens and methanogens identified in the microbiomes. The
884 phylogenetic tree (a and e) and abundance (b and f) of potential exoelectrogens and
885 methanogens. Abundance of CytC (c) and PilA (d) (copies per million reads, average
886 of three replicates). Red asterisk denoted the species capable to produce CH_4 via both
887 acetoclastic and hydrogenotrophic methanogenesis.

888 **Fig. S6** Correlation analysis between methane production and potential
889 exoelectrogens, MAG.138 (a), MAG.142 (b), MAG.161 (c), MAG.6 (d) and MAG.261
890 (e).

891 **Fig. S7** The $\delta^{13}C$-CH_4 and α-value of the feces collected from Shouguang.

892 **Fig. S8** The KEGG gene ortholog diversities of the gut microbiomes. (a) Shannon
893 Index; (b) Inverse Simpson Index; (c) The PCoA analysis of the Bray-Curtis distance
894 based on KEGG gene ortholog abundances.

895 **Fig. S9** Correlation analysis between methane production and acetoclastic
896 methanogens, MAG.271 (a)and MAG.209 (b).

897 **Fig. S10** The abundance of key methanogenic genes.

898

899 **Table Captions**

900 **Table S1** Carbon metabolism pathways.

901 **Table S2.** The abundance and classification of the MAGs.

902 **Table S3.** The abundance of the MAGs and genes encoding the analyzed pathway.

903 **Table S4.** Significant different MAGs among the 4 groups.

904 **Table S5.** The abundance and classification of the MAGs indentified in the
905 samples of Shouguang.

906 **Table S6.** Correlations between the methanogenesis parameters and the
907 compositional parameters at different levels.

908 **Table S7.** Taxonomies corelated with methane production.

909

Highlights

1. Kinetic analysis showed high CH_4 emission in cow feces from early ages.
2. Metagenome-assembled genomes (MAGs) discovered carbon metabolism pathways.
3. Network analysis revealed targeted cooperation in cow feces from different ages.
4. Isotope tracing confirmed the microbiota dominated acetoclastic methanogenesis.

Declaration of interests

☒ The authors declare that they have no known competing financial interests or personal relationships that could have appeared to influence the work reported in this paper.

☐ The authors declare the following financial interests/personal relationships which may be considered as potential competing interests: